Available online at www.sciencedirect.com
SCIENCE DIRECT®
International Journal of Heat and Mass Transfer 49 (2006) 4023–4032
International Journal of HEAT and MASS TRANSFER
www.elsevier.com/locate/ijhmt

Experimental and numerical investigation of premixed acetylene flame

Vukman Bakić, Stevan Nemoda *, Miroslav Sijerčić, Valentina Turanjanin, Branislav Stanković

Laboratory for Thermal and Energy Research, Institute Vinča, P.O. Box 522, 11000 Belgrade, Serbia and Montenegro

Received 31 March 2006
Available online 30 June 2006

Abstract

In this paper, the mean velocity, turbulence intensity and temperature profiles in different cross-sections of premixed acetylene flame are given. A mathematical model for prediction of velocity, temperature and concentration fields of axisymmetric free premixed turbulent flame is presented in this paper. A second-order closure for turbulent reacting flows is used. Special attentions is paid to model behavior with the respect to the prediction correlation coefficients of turbulent diffusion of the scalar components. Conditional and unconditional statistics of the LDA signals were performed using jet and/or air seed. Compared to commonly used unconditional statistics, conditional statistics of velocity fluctuations can give us more data about intensity of turbulent mixing in the flame.

Keywords: Acetylene flame; Second order closure; Premixed; Mixing

1. Introduction

Acetylene premixed flame widely used in metal cutting and material coating, and in many other applications. Experimental investigations of differed flames have been mostly performed with the industrial burners using laser-Doppler anemometry for velocity measurements and thermocouples for temperature measurements, with the aim to reduce noise and to increase combustion efficiency. In several experimental studies [1,2], flow field of the premixed acetylene flame was analyzed. In experiments [2], according to the LDA-velocity information, different regions of the flow field of premixed acetylene–air flame have been established: the flame front, the region of constant flame width (velocity), the developing region, and the fully developed jet flow region. In paper [2] the changes of the premixed acetylene–air flame flow characteristics, which are caused by changes of conditions at the burner exit, changing exit velocity profiles have also been analyzed. Experimental investigations in [3] shows that increasing fuel content in the mixture, velocity and temperature fields are changing considerably. The region of the flame front is characterized by relatively sharp increase in axial velocity followed by axial velocity decrease. Rapid temperature increase caused by combustion brings a flow relaminarization. Adiabatic temperature of the premixed acetylene/air flame is about 2950 K. This high temperature brings an increase in kinematics viscosity and decrease of the *Re* number. In the earlier and recent experimental research of premixed and diffusion flames of gases [4–6], which have lower adiabatic combustion temperatures than acetylene flame, the region of constant velocity was not observed. In the developing region the flow field is similar to the developing region of an isothermal jet. This region is followed by a strongly fluctuating flow region. The velocity along the axis is changing like that of an isothermal jet, self-similarity of the radial velocity profiles is evident [7], and the turbulence intensity is much increased than in other parts of the flow.

Experimental investigations of cold gas entrainment into thermal plasma [8] and into non-premixed propane jet [9] have shown that large difference of density between the hot gas flow and surrounding air is responsible for delay

* Corresponding author. Tel.: +381 112458222x631.
E-mail address: snemoda@vin.bg.ac.yu (S. Nemoda).

0017-9310/$ - see front matter © 2006 Elsevier Ltd. All rights reserved.
doi:10.1016/j.ijheatmasstransfer.2006.04.008

Nomenclature

A	constant in algebraic expression for turbulent dissipation rate [–]
C_μ	constant in effective viscosity expression [–]
C_1	constant in equations for production due to main flow deformation [–]
C_2	constant in equations for production due to main flow deformation [–]
C_s	constant in equations for production due to main flow deformation [–]
$C_{\varepsilon 1}$	constant in equations for energy dissipation [–]
$C_{\varepsilon 2}$	constant in equations for energy dissipation [–]
C_ε	constant in equations for energy dissipation [–]
c_p	specific heat [J kg^{-1} K^{-1}]
E_a	energy of activation [J mol^{-1}]
K_a	absorption coefficient [m^{-1}]
F_x, F_r	radiation fluxes in axial and radial directions [W m^{-1}]
H_r	heat effect of chemical reaction [kJ kmol^{-1}]
h_s	sensitive enthalpy [kJ kg^{-1}]
k	kinetic energy of turbulence [J kg^{-1}]
M_k	molecular mass of species k [kg mol^{-1}]
q_r	heat source due to radiation [–]
R	universal gas constant [J mol^{-1} K^{-1}]
R_k	conversion rate of species y [kg m^{-3} s^{-1}]
r, x	radial and axial coordinate [mm]
r_h	source term in enthalpy equations [–]
S_L	laminar burning velocity [m/s]
S_R	radiation source term [W m^{-3}]
P	pressure [Pa]
T	temperature [K]
U, V	axial and radial mean average velocity [m s^{-1}]
u_{rms}	root of the mean-square velocity fluctuations [m s^{-1}]
u, v, w	fluctuating component of an axial, radial and tangential velocity [m s^{-1}]
y_A	gas components [kg/kg]

Greek symbols

ε	dissipation rate of turbulence [m^2 s^{-3}]
μ	viscosity [Pa s]
ρ	density [kg m^{-3}]
τ^*	time micro-scale [s]
γ	intermittency factor
Ω	mixing factor

Subscripts

fu	fuel
k	chemical species
ox	oxygen

Superscripts

$'$	fluctuations
*	fine structures
^{o}	surrounding

of mixing process, but afterwards it leads to an increase in turbulence level. Conditioning of signal was originally applied for discriminating between turbulent and irrotational fluid elements in non-reacting free turbulent shear flows [10–13], and between reacting turbulent flows and co-flowing air stream [14]. Experimental measurements of conditional and unconditional statistics in premixed flames of various configurations [15–17] are vital to establish relationships between the properties of the two zones, the reactions and the product zones.

The intermittency model [18] assumes that major contributions to flame turbulence are associated with the burnt and unburnt gas states while the contributions from the burning process on a thin surface of the flame front are negligible.

In this paper using conditional and unconditional LDA statistics the mixing processes between acetylene flame and surrounding air in the characteristic region of flame was analyzed in order to reveal physical characteristics of different flame regions. The LDA measurements were performed using three different particle seeding points (1) in premixed unburnt reactants only, (2) in surrounding air only (conditional seeding), and (3) in both reactants and surrounding air (unconditional seeding).

Turbulent premixed flames feature complex interactions between turbulent transport of scalars and chemical reaction as well as a strong coupling between velocity and scalar turbulence. Problems of modeling free flames, and jets in general, arise because of the nonexistence of sharp edges of the physical fields, i.e. of the calculation domain, resulting in unexpected difficulties in solution convergence. Hoping to overcome some uncertainties in calculation of the free premixed flame, in this paper, we have analyzed some specific approaches to solve this problem: (a) flow has been described using elliptical equations; (b) anisotropy of turbulent diffusion of scalar components is introduced; (c) the boundary region of the jet and the surrounding stationary fluid has been implicit treated in the calculations.

In the paper [18] the pressure fluctuation covariance have been studied in detail for six different fuels. Numerical simulations of premixed turbulent flames have the potential to provide versatile cost-effective tools for engineering design in many important applications areas. Moment closure methods have long provided the basis for theoretical models for computations of flows in geometries of practical interest. The principal difficulty associated with such methods concerns the closure of the turbulent transport of

momentum and scalars, the Reynolds stresses and turbulent scalar fluxes.

2. Experimental equipment and flow conditions

The experimental apparatus used in this study has been the same as in [2], except for the new burner with 8 mm inner diameter. Uniform acetylene/air mixture with $\lambda = 1$ (stoichiometric ratio) was supplied to the burner which consists of a long, constant diameter pipe. The length of this burner pipe was $80D$. At the exit of the burner, fully developed turbulent velocity profiles were formed with mean velocity $U_{av} = 15.45$ m/s and $Re = 7862$ and constant turbulent intensity around the burner axis (6%), with increase towards the rim (11%). The laminar burning velocity S_L for stoichiometric mixture was estimated to be 1.83 m/s therefore, u_{rms}/S_L was 0.655. For this exit flow conditions of the acetylene/air mixture, the shape of the flame front was a nearly cylindrical ''flame brush''. This flame is considered to be within the wrinkled laminar region [19,20].

Velocity measurements have been carried out using one-component laser Doppler system consisting of a 15 mW helium–neon laser, a conventional transmission optics including a beam splitter, and a double Bragg cell. Instantaneous velocities in the axial and radial directions have been measured at the same point by rotating the LDA optics by 90°. All measurements have been carried out with a frequency shift of 5 MHz. An angle of 9° was chosen between the axis of the transmission optics and the axis of the receiver optics. With this optical arrangement the dimensions of measuring control volume were $0.16 \times 0.16 \times 1.39$ mm. Frequencies of Doppler signals were obtained by Disa 55L90a counter processor. At each measuring point, 7500 instantaneous velocity samples were recorded and were employed to compute the local mean velocity, turbulence intensity, and the Reynolds turbulent stress. The data were also processed to yield probability density distributions of the instantaneous velocity.

The fuel and surrounding air were seeded with Al_2O_3 particles with mean diameter of 2 μm. Using the estimates from [21] can be shown that such particles can follow the flow velocity fluctuations up to the frequency of 3 kHz. The assumption that the difference between the diffusivities of particles and the fluid may be neglected has been proven valid for large Reynolds numbers [22]. The seeding rates of particles in unburnt mixture and surrounding air were keep constant during the experiment.

3. Modeling of turbulent premixed jet flame by means of second order closure

3.1. Model of the mean flow and turbulence in the flame

Premixed fuel–oxidant mixture is heated by the diffusion radiation and conductive waves from high-temperature combustion products. Combustion is not controlled by the kinetics of chemical reactions, but by the heating rate of the reactive turbulent mixture, so that the turbulent combustion of the premixed gas mixture can be considered primarily as the complex hydrodynamic problem. In reactive flows correlations connected to the density fluctuations appear in the transport equations ($\overline{\rho' u_i}$, $\overline{\rho' u_i u_j}$, $\overline{\rho' t}$ and others). This problem may be overcome using Favre's mass averaging, which eliminates density fluctuation correlations. With Favre averaging, which appears most appropriate for variable density flows, the solution of mean velocity and mean scalar fields requires the density-weighted turbulent stress and turbulent flux of scalar quantities to be determined. Formally, there is nothing new in usage approach based on Favre averaging, but some difficulties arise when comparing calculated to the experimentally obtained flow characteristics. One possibility is solving the conservation equations of turbulent density fluctuations correlations, but, to date, models for these equations have not been adequately developed, although efforts have been made. Models of reactive flows with averaged density yielded acceptable agreement of calculation and experiment, making these models still usable. Also, in our opinion is that the possibilities of this approach are not jet studied enough, specially referring to influence of anisotropic turbulent diffusion of the scalar variables.

The mean velocity field of the free flow can be described by the system of equations derived from Reynold's equations for stationary turbulent flow:

$$\frac{\partial}{\partial x_j}(\rho U_i U_j) = \rho f_i - \frac{\partial P}{\partial x_i} + \frac{\partial}{\partial x_j}\left[\mu \frac{\partial U_i}{\partial x_j} - \rho \overline{u_i' u_j'}\right]; \quad \frac{\partial(\rho U_i)}{\partial x_i} = 0 \tag{1}$$

Closure of the system of Reynolds equations of momentum and continuity equation for stationary turbulent flow of incompressible fluid has been carried out based on the solution of equations for turbulent stress, having the exact form:

$$\begin{aligned} U_k \frac{\overline{\partial u_i u_j}}{\partial x_k} = &- \left[\overline{u_j u_k}\frac{\partial U_i}{\partial x_k} + \overline{u_i u_k}\frac{\partial U_j}{\partial x_k}\right] + \frac{\partial}{\partial x_k}\left(\nu \frac{\overline{\partial u_i u_j}}{\partial x_k}\right) \\ &- \left[2\nu \overline{\left(\frac{\partial u_i}{\partial x_k}\right)\left(\frac{\partial u_j}{\partial x_k}\right)}\right] + \left[\overline{\frac{p}{\rho}\left(\frac{\partial u_i}{\partial x_j} + \frac{\partial u_j}{\partial x_i}\right)}\right] \\ &- \frac{\partial}{\partial x_k}\left[\overline{u_i u_j u_k} + \overline{\frac{p}{\rho}(\delta_{jk} u_i + \delta_{ik} u_j)}\right] \end{aligned}$$

or

$$C_{ij} = G_{ij} + T_{ij} + E_{ij} + \Phi_{ij} + D_{ij} \tag{2}$$

Convective transport (C_{ij}), production due to main flow deformations (G_{ij}), and viscous diffusion (T_{ij}), may be used in their exact form. For modeling of the other terms, approximations based on model described in [23] have been chosen. Redistribution between components of stress (interactions of pressure and flow deformations) is given as

$$\phi_{ij} = -C_1\frac{\varepsilon}{k}\left(\overline{u_iu_j} - \frac{2}{3}\delta_{ij}k\right) - \alpha\left(G_{ij} - \frac{2}{3}\delta_{ij}G\right) - \beta\left(D_{ij} - \frac{2}{3}\delta_{ij}G\right) - \gamma k\left(\frac{\partial U_i}{\partial x_j} + \frac{\partial U_j}{\partial x_J}\right)$$

where $k = \overline{u_ku_k}/2$ is kinetic energy of turbulence, $G = G_{kk}/2$ is production of turbulent kinetic energy, δ_{ij} is Kronecker delta, while

$$G_{ij} = -\left(\overline{u_iu_k}\frac{\partial U_j}{\partial x_k} + \overline{u_ju_k}\frac{\partial U_i}{\partial x_k}\right) \quad \text{and}$$

$$D_{ij} = -\left(\overline{u_iu_k}\frac{\partial U_k}{\partial x_i} + \overline{u_ju_k}\frac{\partial U_k}{\partial x_j}\right)$$

Coefficients α, β and γ are mutually dependent and are determined by coefficient C_2: $\alpha = (8 + C_2)/11$; $\beta = (8C_2 - 2)/11$; $\gamma = (30C_2 - 2)/55$. Viscous destruction is described by the dissipation of turbulent kinetic energy ε, ($E_{ij} = -2/3\varepsilon$), for which the transport equation is solved:

$$U_j\frac{\partial\varepsilon}{\partial x_j} = \frac{\partial}{\partial x_i}\left[\left(\nu + C_\varepsilon\frac{k}{\varepsilon}\overline{u_iu_j}\frac{\partial\varepsilon}{\partial x_j}\right)\right] + C_{\varepsilon1}G\frac{\varepsilon}{k} - C_{\varepsilon2}\frac{\varepsilon^2}{k} \tag{3}$$

Diffusion transport of turbulent stress components is modeled by the expression:

$$D_{ij} = C_s\frac{\partial}{\partial x_k}\left(\frac{k}{\varepsilon}\overline{u_ku_l}\frac{\partial\overline{u_iu_j}}{\partial x_l}\right)$$

Model has six constants, the values of which have been proposed based on the experimental data and numerical optimization, and are given as

$$C_1 = 1.5; \quad C_2 = 0.4; \quad C_s = 0.22; \quad C_{\varepsilon1} = 1.45;$$
$$C_{\varepsilon2} = 1.9; \quad C_\varepsilon = 0.15$$

3.2. Model of the concentration and temperature fields

The model encompasses conservation equations of gas components participating in the process (C_2H_2, O_2, N_2, CO_2, H_2O) and energy equation. To deal with chemical reactions we have solved conservation equations of participating species which, in terms of mass fraction of species A, y_A have general form:

$$\frac{D}{D\tau}(\rho U_k y_A) = -\rho\frac{\partial}{\partial x_k}(\overline{u_ky'_k}) + \frac{\partial}{\partial x_k}\left(D\frac{\partial y_A}{\partial x_k}\right) + r_A \tag{4}$$

The equations have been solved by means of conservation equations for Reynolds fluxes $\rho\overline{u_iy'}$ which are of the modeled form:

$$\frac{D}{D\tau}(\overline{u_iy'}) = -\left(\overline{u_ku_i}\frac{\partial y}{\partial x_k} + \overline{u_ky'}\frac{\partial U_i}{\partial x_k}\right) - C_{\varepsilon1}\overline{u'_ky'}\frac{\partial U_i}{\partial x_k} - C_{\varepsilon2}\frac{k^2}{\varepsilon}\left(\frac{\partial\overline{u_iy'}}{\partial x_j} + \frac{\partial\overline{u_jy'}}{\partial x_i}\right) + r_y \tag{5}$$

production and destruction of particular components in the mixture are shown as part of the source terms of the equations, through the kinetic relations and corresponding stoichiometric ratios. Basic chemical equation of acetylene combustion is as follows:

$$C_2H_2 + 2.5O_2 = 2CO_2 + H_2O + H_r,$$

where $H_r = 1.25\times10^6$ kJ kmol^{-1} is the heat effect of chemical reaction. Heat transfer in the flame was considered through the equation of sensitive enthalpy $h_s = \sum_l y_l C_{p,l}T$. Enthalpy equation has the same form as Eq. (4), but with the source term equal:

$$r_h = U\frac{\partial P}{\partial x} + V\frac{\partial P}{\partial r} + q_r + r_{\text{fuel}}H_r \tag{6}$$

where terms $r_{\text{fuel}}H_r$, describe the heat effect of the chemical reaction in the flame. The term q_r, on the right hand side of Eq. (6) represent the heat source due to the radiation. For the radiation heat transfer, six flux model [24], reduced for axial-symmetric case of purely emission–absorption radiation to two equations of the diffusion type for radiation fluxes, in axial ($F_x = I_x + J_x$) and radial ($F_r = I_r + J_r$) directions were used:

$$\frac{\partial}{\partial x}\left(\frac{1}{k_a}\frac{\partial F_x}{\partial x}\right) = K_aF_x - \frac{1}{3}K_aI_b;$$
$$\frac{1}{r}\frac{\partial}{\partial r}\left(\frac{1}{k_a}r\frac{\partial F_r}{\partial r}\right) = K_aF_r - \frac{1}{3}K_aI_b \tag{7}$$

where I_b is the emission power of the black body, and $K_a = -(1/L)\ln(1 - e_g)$ is the absorption coefficient of the medium. In the energy equation heat source due to the radiation is described by the term:

$$q_r = \operatorname{div}\vec{Q}_r = K_a\left(F_x + F_r - \frac{2}{3}I_b\right)$$

Reynolds fluxes $\rho\overline{u_ih'_s}$ are modeled in same way as $\rho\overline{u_iy'}$ in Eq. (5).

3.3. Combustion model

Although this kind of flame has been investigated, but available data still suffer from some incertitude and contradictions [25]. Acetylene oxidation rate determined by the Arrhenius relation [26]: $r_{ch} = AX_{fu}^{0.5}X_{ox}^{1.25}\rho^{1.75} > \exp(-E/RT)$, where $A = 9.5\times10^{14}$ and $E/R = 1.51\times10^4$ K is much grater than the combustion rate in the real flame. Several different models proposed in order to determine real combustion rate have been reviewed in e.g. [27]. Proposed model of combustion rate is base on an eddy dissipation concept [28,29], but including chemical kinetics into fine structures too. Basic assumption of the model used here is that chemical reactions take place when reactants are mixed at molecular scale in isolated regions whose entire volume is a small fraction of the fluid elements. These regions are occupied by the structures that represents end of cascade eddy dissipation process, whose characteristic dimensions are of the same order of magnitude as the Kolmogorov microscale. Consideration of the contact probability of fluctuating reactants was substituted by consideration of mixing on molecular level inside fine turbulent

structures. Calculation of the overall combustion rate is thus reduced on the determination of participation fine structures in turbulence, and afterwards on analysis of processes in fine structures. In proposed model both, the chemical kinetics and molecular mixing, are considered at the same time, while in similar models the chemical kinetics is treated separately, or is neglected at all. Simultaneous influence of chemical kinetics and turbulent mixing on the combustion rate is attained by treating fine structures like ideal chemical reactors.

Based on the mass balance for species "i" in the fine structures and surrounding fluid, and including chemical kinetic rate, source term can be expressed as: $r_i^* = \rho^*(y_i^o - y_i^*)/\tau^* = r_{\mathrm{ch}}^*$ where y_i^o and y_i^* are mass fractions of species "i" outside and inside the fine structures respectively and $r_{\mathrm{ch}}^* = k_{\mathrm{ch}}\rho^{*(a+b)}y_i^{*a}y_j^{*b}$ chemical reaction rate. If the total mass m, is equal to the sum of masses in fine structures m^* and surrounding m^o: $m = m^* + m^o$, then mass fraction occupied by fine structures is defined as: $\gamma^* = m^*/m$ and mean mass fraction of deficient species "i" in control volume: $y_i = y_i^*\gamma^* + y_i^o(1-\gamma^*)$. Taking into account the stoichiometric relation for chemical reaction, mass fraction of the second reactant—"j" in the turbulent fine structures is defined by : $y_j^* = y_j - s_t(y_i - y_i^*)$. When "$i$", which is deficient species in control volume, represents fuel $s_t = s_{\mathrm{fu}}$ and when "i" represents oxygen, $s_t = 1/s_{\mathrm{fu}}$. Considering these relations, set of two equations with two unknowns (mass fraction y_i^* and conversion rate r_i^* in fine structures) can be formed:

$$\frac{\rho^*(y_i - y_i^*)}{\tau^*(1-\gamma^*)} = k_o \mathrm{e}^{-\frac{E_a}{RT}} y_i^{*a}[y_j - s_t(y_i - y_i^*)]^b;$$
$$r_i^* = \frac{\rho^*(y_i - y_i^*)}{\tau^*(1-\gamma^*)} \tag{8}$$

Reaction rate r_i^* corresponds to the mass fraction occupied by fine structures and reactant "i" represents "deficient species". Taking this into account, total reaction rate in the case of finite chemical reaction rate, can be expressed by

$$r_{\mathrm{fu}} = r_i^*\gamma^* \text{ for } \frac{y_{\mathrm{ox}}}{s_{\mathrm{fu}}} \geqslant y_{\mathrm{fu}} \wedge r_{\mathrm{fu}} = \frac{r_i^*\gamma^*}{s_{\mathrm{fu}}} \text{ for } \frac{y_{\mathrm{ox}}}{s_{\mathrm{fu}}} < y_{\mathrm{fu}} \tag{9}$$

Time scale for the fine structures, as mentioned, corresponds to the Kolmogorov time scale: $\tau^* = a_\tau\sqrt{\nu/\varepsilon}$. Mass fraction occupied by fine structures (γ^*) can be obtained as the ratio between Kolmogorov microscale and bulk mixing time scale: $\gamma^* = \tau^*/\tau_{\mathrm{m}}$. If we suppose that bulk mixing time scale is proportional to the turbulent macro scale, the ratio of micro and macro scales is as follows: $\tau^*/\tau^{\mathrm{m}} \propto \sqrt{\nu/\varepsilon}/(1/u) = R_t^{-0.5}$ and mass content of the fine turbulent structures can be written by the expression: $\gamma^* = a_\tau\sqrt{\nu\varepsilon/k^2}$. Taking into account that the fine structures, as well as Kolmogorov microscale, are responsible for the dissipation of turbulent energy, it can be assumed $a_\tau = 1$. Comparing the numerical results with our experimental data, $a_\gamma = 0.92$ is accepted.

3.4. Thermodynamic and transport properties

With density of the components given by ρ_i ($\rho_i = M_iP/RT$), mixture density is defined as: $\rho = \sum_i y_i/\sum_i(y_i/\rho_i)$. By using constants $l_{1,i}i$ $l_{2,i}$ determined from the referent tables, the molecular viscosity of the components is: $\mu_i = l_{1,i}/(1 + l_{2,i}/T)$. Molecular viscosity of the mixture is determined using the equation: $\mu = \sum_i\left(X_i\mu_i/\sum_j X_j\Phi_{ij}\right)$, where: X_i and X_j are mole fractions and $\Phi_{ij} = 0.35(1 + M_i/M_j)^{-0.5}[1 + (\mu_i/\mu_j)^{0.5}(M_j/M_i)^{0.25}]^2$. Specific heat capacity of the gas components is determined using fourth order regression: $C_{p,i} = a_i + b_iT + c_iT^2 + d_iT^3 + e_iT^4$, and for the mixture using: $C_p = \sum_i C_{p,i}y_i$. Thermal diffusion coefficient $\alpha = \lambda/\rho C_p$ is determined as the ratio of the viscosity and the Prandtl number $\sigma_h = C_p\mu/\lambda$; $\alpha = \nu/\sigma_h$.

4. Experimental and numerical results

4.1. Axial mean flow velocity, turbulence intensity, and temperature profiles for stoichiometric flame

Fig. 1 show the experimental data and computation results for the mean velocity Fig. 1(a) and turbulence intensity and (b) changes along the flame axis. Considering the complexity of the problem, agreement is good. The region of flame front (I) ends approximately $3D$ downstream of the burner exit; temperature increase, i.e. density decrease is dominant compared to the flow deceleration due to the shear stresses at the front of the flame, leading to the acceleration of the flame jet in this region, which is less pronounced in the model than in the experimental data. It must be noticed that this effect could not be obtained by use of turbulent viscosity model. The region of constant velocity (II) ends at $8.5D$ downstream of the burner exit, from where the ambient air penetrates to the flame centerline. Measurements conditioned on the surrounding air could not have been carried out for axial distances $x/D < 8.5$. In this region, the surrounding air did not penetrate to the flame axis. For axial distances $x/D > 8.5$ the mean axial velocity of fluid in the jet is considerably higher than the mean axial velocity of fluid originating from the surrounding air. Large volumes of entrained cold air have much higher density and, thus, greater inertia than the combustion products. With intensification of mixing processes between flame and surrounding air the difference between velocity of fluid originating from the flame and the fluid from surrounding air disappears, approximately at $x/D > 25$.

Transition from the developed region (III) to fully developed region (IV) is characterized by an intense mixing of combustion products with the surrounding air, which is accompanied by a sudden fall of temperature and radiation intensity. The eddies in the flow are continually breaking down into the smaller eddies, while diffusion is taking place, at molecular level, at all eddy boundaries. The jet becomes fully turbulent in region IV of sharply increasing turbulence, while eddies of surrounding air continue to

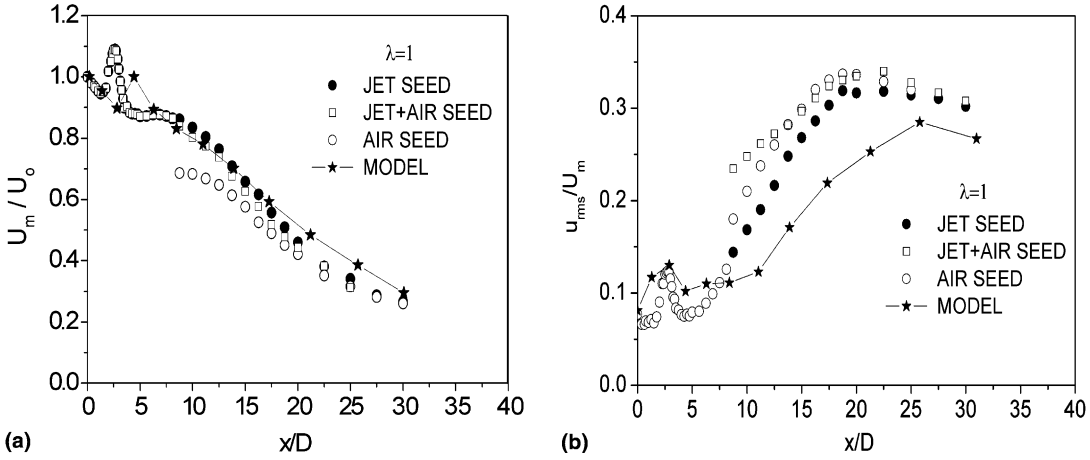

Fig. 1. Mean axial velocity (a) and turbulence intensity (b) along the flame axis.

be engulfed into flame, further reducing velocity. Velocity change along the flame axis is also influenced by the velocity values at the nozzle outlet. High velocity at the nozzle outlet causes wider flame front. This is probably due to the dependence of the flame spreading rate on the velocity of the incoming gas flow [30]. The mentioned influences on the flow characteristics of the flame are hard to express quantitatively, being that every flame is unique in its own.

Turbulence intensity distribution along the flame axis, also both for conditional and unconditional seeding, shown in Fig. 1(b), has been normalized using the local mean velocity at the axis. Just downstream of the burner exit, turbulence intensity is $T_u = u_{rms}/U_m$ approximately constant. It stays constant until the flame front is reached. At the flame front, the maximum turbulence intensity occurs at the same point where the mean velocity at the flame axis increases. Then T_u considerably decreases in constant velocity region characterized by relaminarization of flow and absence of mixing process between combustion products and surrounding air. Considering the complexity of the problem, computation results, despite the obvious deviations, can be accepted as a successful illustration of the turbulence intensity.

Large density difference delays the mixing process. With downstream increase in turbulence intensity the difference between conditional and unconditional seeding of particles disappears.

Fig. 2 shows isotherms. Measured values are limited to the temperature of 1773 K for $\lambda = 1$ (stoichiometric ratio), because a maximal of measuring range of thermocouple is 1950 K. The region of constant velocity II, $3 < x/D < 8.5$ (see Fig. 1(a)), around the flame axis is the region of high temperature, which is a reason for drastic increase of viscosity, which together with acceleration gives as a result the stream relaminarization beyond the flame front and formation of constant velocity region. Downstream of constant velocity region, with intensification of the mixing processes between combustion products and surrounding air, temperature decreases and usual flow development in the

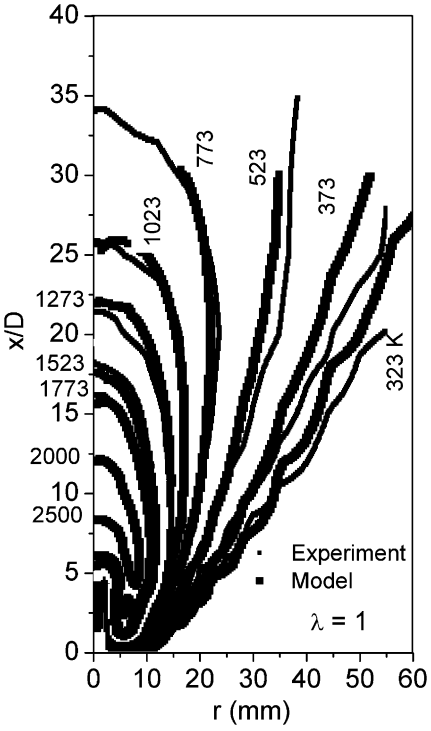

Fig. 2. Isotherms in the acetylene flame.

jet occurs, with gradual decrease of velocity at the jet axis. From the figure it can be seen that near the nozzle exit the flame temperature increase is sharper at the flame edge than inside the flame. This may seem unexpected, but it can be explained by the violent reaction with oxidant in excess at the flame edge, and by the longer reaction time due to the lower velocity at the point.

Measured axial mean velocity (U), radial mean velocity (V), and turbulence intensity for $x/D = 5$, for conditional and unconditional statistics are shown in Fig. 3. The axial and radial mean velocities are also normalized by the velocity value at the axis U_m. Radial coordinate is normalized by the distance from the flame axis, b, where the unconditional axial mean velocity is half the unconditional maximum

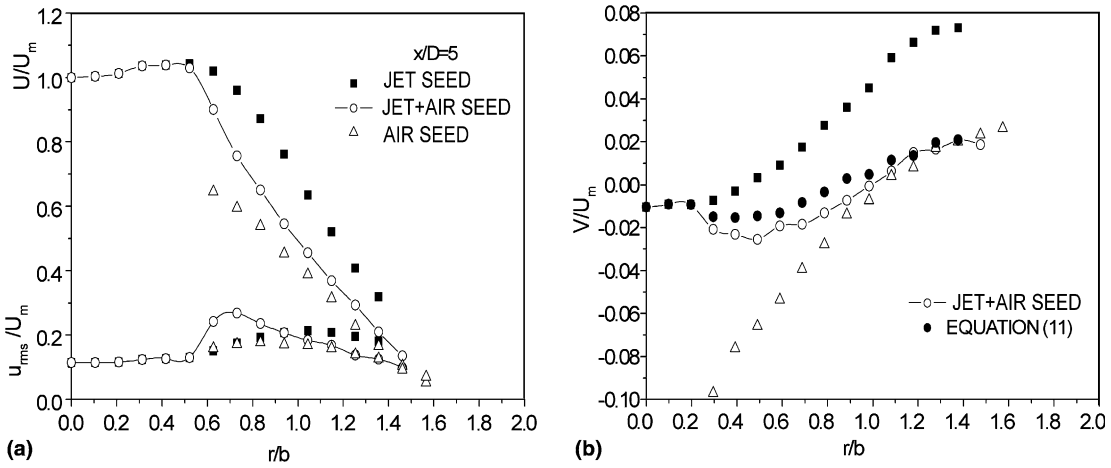

Fig. 3. Profiles of mean axial velocity, turbulence intensity (a) and radial velocity and turbulence intensity (b) at $x/D = 5$.

axial velocity at the flame axis. The turbulence intensity distributions along the axial velocity component and radial mean velocity are normalized using the local mean velocity U_m.

For $x/D = 5$, mean axial and radial velocities (Fig. 3(a) and (b)) for conditional jet seeding and unconditional seeding, in central region around flame axis have constant values. In this region there is no mixing between combustion products and surrounding air. Decrease of mean axial velocity in cross section $x/D = 5$ starts at the point $r/b = 0.6263$ ($r = 6$ mm) where the mixing process between surrounding air and combustion products begins (this point can be used as start of the constant velocity region). As Fig. 3(a) shows, mean axial velocity conditioned on air seed and on jet are different. The mean axial velocity conditioned on jet is higher than the mean axial velocity conditioned on air. Therefore, in general, fluid originating from the surrounding air has lower velocity than the fluid originating from combustion products. The values of unconditioned mean axial velocity near the flame axis are close to the values of mean axial velocity conditioned on jet seed.

At axial distance $x/D = 8$ [31], the width of the constant velocity region is less than at distance $x/D = 5$. The boundary of this region becomes smaller by $r/b = 0.3$ ($r = 3$ mm). The character of velocity profiles at $x/D = 8$ is similar to the velocity profiles at $x/D = 5$.

The profiles of axial velocity for $x/D = 15$ [31] have a shape characteristic for fully developed region of an isothermal jet. At this distance there is no constant velocity region.

The U/U_m velocity distributions conditioned on jet seed and unconditioned at axial distances $x/D = 5$ and $x/D = 8$ [31] are low and constant in the region where there is no mixing between surrounding air and combustion products. This points to the fact that the measurements were based mainly on the fluid particles originating from the jet. The turbulence intensity is increased in the region $0.5 < r/b < 1.25$, where the mixing of the jet fluid and surrounding air takes place, coinciding with the region of maximum velocity gradient.

The mean radial velocities for unconditional and conditional seeding at axial distances $x/D = 5$ are shown in Fig. 3(b). The profiles of radial mean velocity indicate entrainment of surrounding air (negative values) and outward expansion of gas originating from the jet (positive values).

4.2. Mixing factor and probability density distributions

For conditional and unconditional statistics, the following relations hold true:

$$U = \Omega U_{\text{jet}} + (1 - \Omega) U_{\text{air}} \tag{10}$$

$$V = \Omega V_{\text{jet}} + (1 - \Omega) V_{\text{air}} \tag{11}$$

Eqs. (10) and (11) are formally identical with equations describing the relation between intermittency factor γ and the mean velocity, which have been obtained by averaging in the turbulent and non-turbulent regions using hot-wire anemometer [11]. Similar definition was used in [12] to describe the intermittency of unburnt reactants and combustion products at the same point. The passive scalar Ω in our case is defined as the probability that the fluid originating from the jet is present at any given point. Hence, factor $(1 - \Omega)$ is the probability that fluid originating from the surrounding air is present at that same point. Generally γ and Ω need not be identical. The Ω in the cross sections $x/D = 5$, 8, 10, and 15 are shown in Fig. 4(a).

The sharp decrease of Ω between $r/b = 0.5$ and 1.0 in the flame cross section at $x/D = 5$ indicates that in this case the mixing process is restricted to a very narrow region. In the downstream cross sections the mixing process takes place in a wider region occupying virtually the entire flame cross section at $x/D = 15$.

The mixing factor (passive scalar) Ω obtained from Eqs. (10) and (11) subsequently used to calculate the values of unconditional radial velocity component, from the

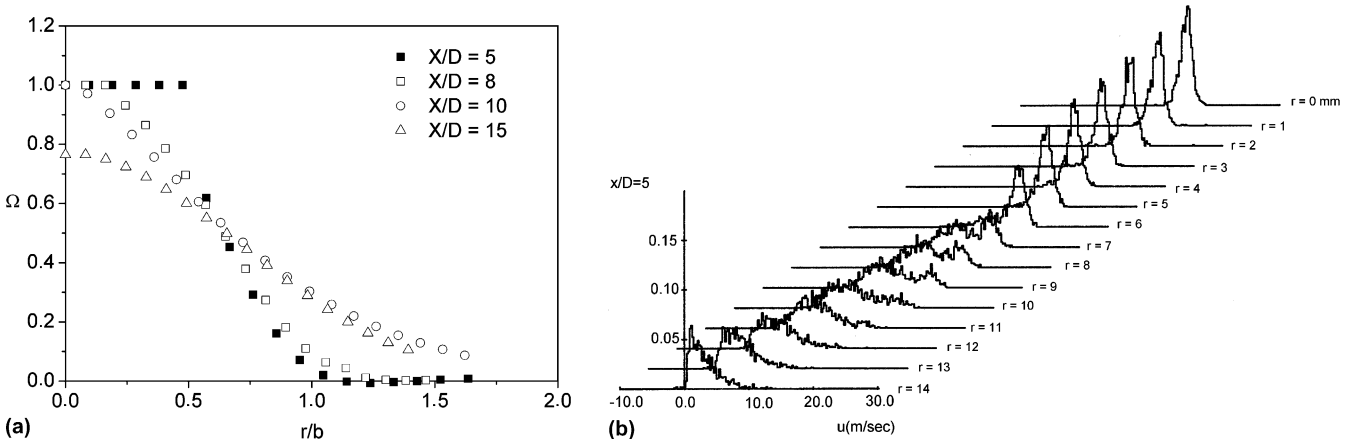

Fig. 4. Mixing factor in the flame (a) and the Pdf(u) distribution in the flame at $x/D = 5$ (b).

measured conditional ones, using Eq. (11), Fig. 3(b). The agreement between air + jet seed measured and calculated (using Eq. (11)) unconditional radial mean velocity is good, keeping in mind that U and V components have been measured in separate experiments.

An insight into the statistical properties of the instantaneous velocities in acetylene flame was gained from their corresponding probability density distributions Pdf. Fig. 4(b) shows Pdf(u) in the flame cross section at the axial distance $x/D = 5$ for unconditional seeding. The turbulence intensity is constant for radial distances $r \leqslant 6$ mm, where there is no mixing between surrounding air and combustion products. For distances $6 < r < 11$ all velocity Pdf(u) are bimodal with two separated maximums corresponding to the combustion products and surrounding air. The bimodal shape of Pdf(u) disappears closer to the flame edge, where the fluid from the surrounding air dominates. At $x/D = 8$ [31], constant velocity region extends to the $r = 3$ mm distance. In this region the probability density functions are similar, illustrating the fact that turbulence intensity has constant value (see Fig. 3(a)). On radial distances $y > 3$ mm, mixing process between combustion products and surrounding air is taking place. The Pdf(u) in this region have bimodal shape which disappears with approach to the jet edge. Because of the turbulization of fluid flow and the decrease in density difference in downstream cross sections, the breakdown of large eddies happens, and the mixing between combustion products and the surrounding air is intensified. The Pdfs(u) at the axial distance of $x/D = 15$ [31] cannot show bimodal shape.

The following relations hold true for unconditional and conditional probability density functions:

$$\mathrm{Pdf}(u) = \Omega \mathrm{Pdf}(u)_{\mathrm{jet}} + (1 - \Omega)\mathrm{Pdf}(u)_{\mathrm{air}} \tag{12}$$

$$\mathrm{Pdf}(v) = \Omega \mathrm{Pdf}(v)_{\mathrm{jet}} + (1 - \Omega)\mathrm{Pdf}(v)_{\mathrm{air}} \tag{13}$$

If the values for mixing factor Ω calculated from Eqs. (10) and (11) are substituted into Eqs. (12) and (13), then one Pdf may be calculated based on the other two. Fig. 5 shows

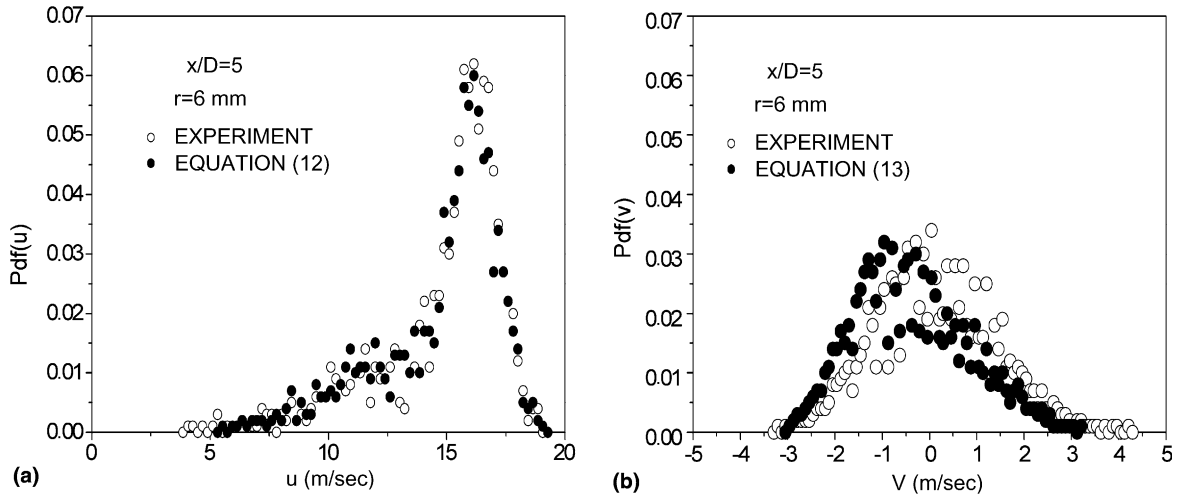

Fig. 5. Comparison of Pdf measured experimentally and calculated using Eqs. (12) and (13).

Pdfs(u) and Pdfs(v) at $x/D = 5$ and at the radial distance $r = 6$ mm, measured with unconditional seeding and calculated based on the measured Pdfs for conditional seeding. Measured and calculated Pdfs are well compatible with each other and confirm that the relationship exists between them, in the form (12) and (13). At other positions there is also a good compatibility between Pdfs obtained from the experiments and by using Eqs. (12) and (13) [31].

4.3. Calculated species concentration

In Fig. 6, changes of basic active chemical components mass concentrations in the flame have been shown. For the illustration of combustion process in Fig. 7(a) and (b), calculated radial profiles of oxygen and carbon dioxide concentration on particular axial locations are shown. From these figures (and also from the profiles of other components, which have not been shown), the border of the flame front in radial distance as well as entrainment of the fresh air in the jet beyond the flame front can be noticed.

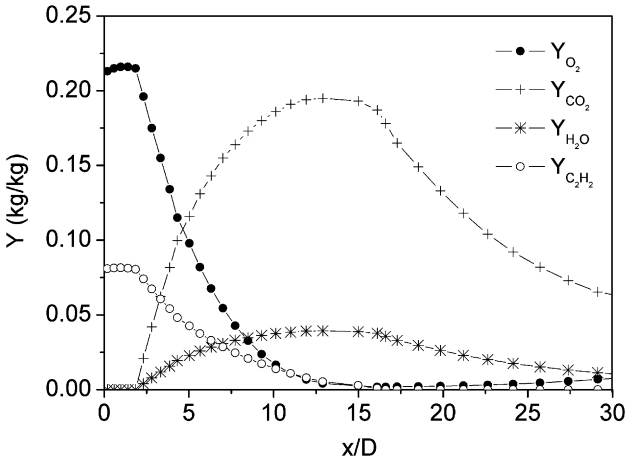

Fig. 6. Calculated distributions of reactive species concentration.

5. Conclusions

The described model is based on solving the elliptic partial differential equations, representing a qualitatively different approach from the some modeling of the free premixed flames based on the parabolic differential equations. Non-conventional boundary conditions for free flows, which should make the model agree better with the physical nature of the problem, have also been incorporated into the model. Reducing the complexity of the combustion problem is often achieved by assuming that the turbulent mass diffusion coefficient are the same for all components. We found that introduction flux–stress significantly improved the results quality in comparison to k–ε model. The application of Re–stress model provides a powerful tool for improving the accuracy of prediction free flames.

The results of LDA measurements for three different particle seeding points (in premixed unburnt reactants only, in surrounding air only and in both reactants and surrounding air) show that this seeding technique provides a useful marker for fluid elements originating from the combustion products and surrounding air. The resulting conditional and unconditional velocity statistics provide valuable information on details of the mixing process between these two fluids. In the region of the flame front and constant mean velocity, large differences between both axial and radial velocity components of cold eddies of surrounding air and hot eddies of combustion products have been detected. Due to the high viscosity in this region the turbulence intensity is very low. This also confirms that large density difference delays and suppresses the mixing process in this region. In this flame region the area where mixing process takes place is very narrow.

These flow characteristics indicate that downstream of the flame front a sort of potential core is formed, characterized by constant mean velocity, low turbulence intensity, and weak mixing in the narrow region on the boundary with surrounding air. An analysis of flow in this region has shown that this flow may be treated as turbulent flow

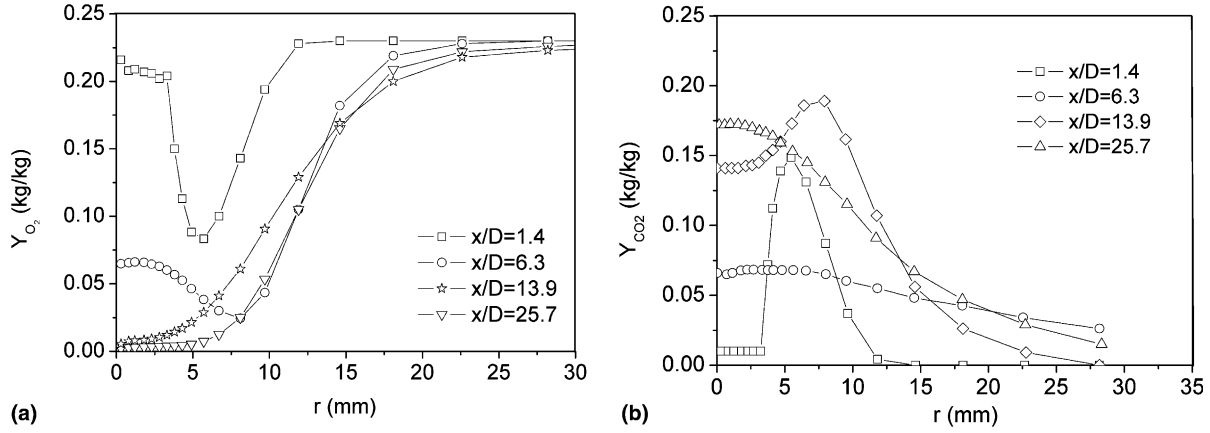

Fig. 7. Development of the oxygen (a) and carbon dioxide (b) concentration profile.

in pipe. From this we can conclude that relaminarization behind flame front is incomplete.

Downstream from this apparent potential core, with diminishing density difference, an intense mixing takes place, with sharp increase in turbulence intensity. It has been shown that the mixing factor obtained from axial velocity measurements, defined in a similar way to intermittency factor, can be used for analyzing the mixing process. This passive scalar can also be used to establish relations between conditional and unconditional mean velocities, both for axial and radial components.

The model provides insight into the structure and aerodynamics characteristics of the flame. A modern approach to the modeling of combustion requires attention to be paid to the turbulent density fluctuations, which means the development of models with Favre's averaging or the development of models for turbulent correlations with density fluctuations. Also, what may be interesting are the flux-stress models for flows with combustion. A more detailed analysis may also be required for the modeling of the chemical reactions, especially formation of char in the flame.

References

[1] S. Oka, P. Radulovic, M. Matovic, V. Pislar, P. Stefanovic, in: Transfer Processes in One and Two-Phase Flows, Novosibirsk, Academy of Sciences USSR, Siberian Branch, 1986, pp. 112–125.

[2] M. Matovic, S. Oka, F. Durst, Structure of the mean velocity and turbulence in premixed axisymmetric acetylene flame, J. Fluids Eng., Trans. ASME 116 (1994) 631–643.

[3] V. Bakic, S. Belosevic, Fuel–air ratio influence on mixing processes between premixed acetylene flame and surrounding air, Thermal Sci. 4 (2) (2000) 33–40.

[4] J.P. Sislian, L.-Y. Jiang, R.A. Cusworth, Laser Doppler velocimetry investigation of the turbulence structure of axisymmetric diffusion flames, Prog. Energy Combust. Sci. 14 (1988) 99–146.

[5] P.A. Libby, S. Sivasegaram, J.H. Whitelaw, Premixed combustion, Prog. Energy Combust. Sci. 12 (1986) 393–405.

[6] P. Stroomer, Turbulence and OH structures in flames, Ph.D. thesis, Delft, The Netherlands, 1995.

[7] M. Matovic, Experimental investigation of the flow field of premixed turbulent flame using LDA, M.Sc. thesis, University of Belgrade, Mech. Eng. Faculty, Yugoslavia, 1989.

[8] E. Pfender, J. Fincke, R. Spores, Entrainment of cold gas into thermal plasma jets, Plasma Chem. Process 11 (4) (1991) 529–537.

[9] R.W. Schefer, V. Hartman, R.W. Dibble, Conditional sampling of velocity in a turbulent nonpremixed propane jet, AIAA J. 25 (1986) 1318–1328.

[10] H.A. Becker, H.C. Hottel, G.C. Williams, On the light-scatter technique for the study of turbulence and mixing, J. Fluid Mech. 30 (2) (1967) 259–275.

[11] R.A. Antonia Prabhu, S.E. Stephenson, Conditionally sampled measurements in a heated turbulent jet, J. Fluid Mech. 70 (3) (1975) 455–470.

[12] R. Cheavray, N.K. Tutu, Intermittency and preferential transport of heat in a round jet, J. Fluid Mech. 88 (1) (1978) 133–151.

[13] R.W. Bilger, R.A. Antonia, K.A. Sreenivasan, Determination of intermittency from the probability density function of passive scalar, Phys. Fluids 19 (10) (1976) 471–1485.

[14] J.B. Moss, Simultaneous measurements of concentration and velocity in an open premixed turbulent flame, Combust. Sci. Technol. 22 (1980) 119–135.

[15] R.K. Cheng, I.G. Shepherd, Intermittency and conditional velocities in premixed conical turbulent flames, Combust. Sci. Technol. 52 (1987) 353–375.

[16] R.K. Cheng, Conditional sampling of turbulence intensities and Reynolds stress in premixed turbulent flames, Combust. Sci. Technol. 41 (1984) 109–142.

[17] P.A. Libby, N. Chinger, J.C. LaRue, Conditional sampling in turbulent combustion, Prog. Energy Combust. Sci. 8 (1989) 203–231.

[18] P. Domingo, K.N.C. Bray, Laminar flamelet expressions for pressure fluctuation terms in second moment models of premixed turbulent combustion, Combust. Flame 121 (2000) 555–574.

[19] R.K. Cheng, I.G. Shepherd, Interpretation of the conditional statistics in open oblique premixed turbulent flames, Combust. Sci. Technol. 49 (1986) 17–35.

[20] R. Borghi, On the structure of turbulent premixed flames, in: C. Bruno, C. Casci (Eds.), Recent Advances in Aeronautical Science, Pergamon, 1984.

[21] R.D. Ballal, The structure of premixed turbulent flame, Proc. R. Soc. London A 367 (1979) 485–502.

[22] F. Durst, A. Melling, J.A. Whitelaw, Principles and Practice of Laser-Doppler Anemometry, Academic Press, London, 1976.

[23] B.E. Launder, G.J. Reece, W. Rodi, Progress in the development of a *Re*–stress turbulence closure, J. Fluid Mech. 68 (3) (1975) 537–566.

[24] C.T. Chu, S.W. Churchill, Numerical solution of problems in multiple scattering of electromagnetic radiation, J. Phys. Chem. 59 (1955) 855–863.

[25] P.A. Libby, F.A. Williams (red), Turbulent Reacting Flow, Academic Press, London, 1995.

[26] R.H. Essenigh, E.M. Suuberg, The role of volatiles in coal combustion, in: Proceedings of NATO Advanced Research Workshop on Fundamental of the Physical Chemistry of Pulverized Coal Combustion, Les Ares, 1986.

[27] E.E. Khalil, Modeling of Furnaces and Combustors, Abacus Press, London, 1982.

[28] S. Byggstoyl, B.F. Magnuson, in: Proceedings of the 4th Symposium on Turbulent Shear Flows, Karlsruhe, 1983, pp. 10.32–10.38.

[29] R. Driscoll, L. Kennedy, in: Proceedings of the 19th Symposium on Combustion, Combustion Institute, Pittsburg, 1982, pp. 387–392.

[30] D.R. Ballal, Studies of turbulent flow–flame interaction, AIAA 24 (1) (1986) 1148–1154.

[31] V. Bakić, Investigation of a turbulent flame structure using conditional signal sampling, M.Sc. thesis, Faculty of Mechanical Engineering, Belgrade, 1997.